EXPERIMENTAL STUDY FOR IMPROVING DUCTILITY OF EARTHQUAKE-DAMAGED RC PIERS

(Translation form Proceeding of JSCE, No. 578/V-37, Nov. 1997)


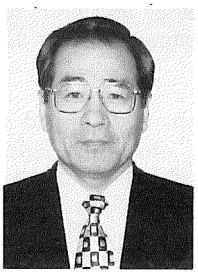

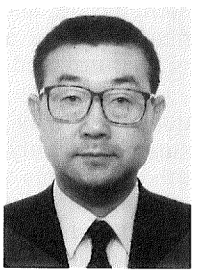
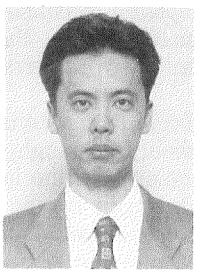

Kenji KOSA Hisanori OTSUKA Junichi HOSHIKUMA Kyoichi SASAKI Hiroshi SHIMBO

Experiments using 1/6-scale models were conducted on earthquake-damaged RC piers on the Kobe route of the Hanshin Expressway to confirm that various proposed retrofit methods can attain the intended high deformation capacity of over 5 δ_y The retrofit methods compared were steel plate jacketing, RC jacketing, a combination of steel and RC jacketing, and the reconstruction of RC piers. Nonlinear RC analysis was also carried out using a fiber model to allow a quantitative evaluation of the strengthening effect of these methods.
Both experimental and analytical results demonstrated that all four retrofit methods can achieve a large ductility increase well exceeding the level demanded by the Specifications for Highway Bridges. It was also found that post-installed anchors, which are driven in to unify the pier with the footing, would not be a weak point under earthquake loading.

Keywords: ductility, load-deflection, non-linear analysis, retrofitting

---

Kenji Kosa, a member of the JSCE and ASCE, is an associate professor in the Department of Civil Engineering at the Kyushu Institute of Technology. Before joining the faculty in 1999, he was a senior highway engineer at the Hanshin Expressway Public Corporation in Osaka. He obtained his Ph.D. from the University of Michigan, Ann Arbor in 1988. His main research interests are the analysis and design of concrete structures.

Hisanori Otsuka is a professor in the Department of Civil and Structural Engineering at the Kyushu University. He received his Dr. Eng. from Kyushu University in 1979. He worked for the Division of Earthquake Engineering in the Public Works Research Institute, Ministry of Construction during 1991 and 1996. He is a member of the JSCE, JCI, JSSC and IABSE.

Junichi Hoshikuma is a senior research engineer in the Earthquake Engineering Division at the Public Works Research Institute, Ministry of Construction. He obtained his Dr. Eng. from Kyushu University in 1998. His research interests relate to the seismic design of concrete bridges and underground structures. He is a member of the JSCE.

Kyoichi Sasaki is a section manager at Yachiyo Engineering Co., Ltd. He obtained his BE in transportation engineering from Nihon University in 1973. His research interest is the seismic design and retrofit of concrete structures. He is a registered consulting engineer and a member of the JSCE and JCI.

Hiroshi Shimbo is an engineer at Civil Engineering Design Division of Kajima Corporation. He obtained his MS in civil engineering from Kyushu University in 1990. He is a registered engineer. His research interest is the seismic design of concrete structures.

---

1. INTRODUCTION

The Great Hanshin Earthquake of Jan. 17, 1995 caused tremendous damage to the structures of the Hanshin Expressway's Kobe Route running between the cities of Osaka and Kobe. The severe damage included the collapse of girders from piers. RC piers that suffered significant damage were removed and new piers were constructed their place. Piers with relatively light damage were repaired, seismically strengthened, and returned to service. Footings and piles found to be virtually unaffected by the earthquake were all reused with minor repairs or even as is. Footings were unified with piers using post-installed anchors [1].

Regarding reconstruction of heavily damaged RC piers, it was determined that the new piers should be tough structures - not only strong but highly ductile - to withstand at least the seismic intensity of the last earthquake. This was documented in "Specifications for the Retrofit of Bridges Damaged by the Great Hanshin Earthquake (Retrofit Specifications)" as meaning that the lateral confinement of piers should be increased by reinforcement to provide sufficient ductility [2].
Meanwhile, the RC piers along the Kobe route are relatively old structures designed by the standards of 1964 or 1971, when stipulations were yet to be made on the cut-off of main reinforcement or the checking of ultimate lateral strength. Therefore, seismic strengthening was needed even for piers that survived the earthquake with minor damage. Thus, we had to find ways to satisfy the ductility demands of not only new piers but also other surviving piers.

We were unable to utilize past investigations on bridge ductility as a direct reference for our retrofit program because investigation parameter ranges - hoop tie ratios up to 0.4% and ductility up to 5 δ_y [3] [4] [5] [6] - were too limited for our intended ductility increase. Therefore, for these structures where the ductility demand was greater than 5 δ_y, new experiments were needed.

Thus, using models simulating the RC piers on the Kobe route that suffered earthquake damage, experiments were carried out to verify that the proposed strengthening methods, namely steel jacketing, RC jacketing, steel + RC jacketing, and RC reconstruction, could provide the required deformation capacity. The experimental results were compared with analytical results using load-displacement curves to see if a quantitative numerical evaluation of strengthening effect was feasible. The load-displacement curves were obtained using, as the stress-strain model of concrete, the Public Works Research Institute (PWRI) model prescribed in the Retrofit Specifications and the Kent-Park model, which has been used for such investigations internationally. Lastly, using a fiber model as conventionally used for such analysis, reverse cyclic loading analysis was performed on the strengthened piers, and their load-displacement behavior was evaluated.

2. APPROACH TO RETROFIT DESIGN

Most bridge piers on the Kobe route were constructed in the late 1960s based on the Specifications for Highway Bridges enforced in 1964. In that standard, the design horizontal seismic coefficient was 0.2. The allowable shear stress for concrete was 7 kgf/cm^2. This was considerably greater than the 4.2 kgf/cm^2 allowed after 1971. In those days, designers commonly thought that the concrete cross section was enough to provide sufficient shear strength. As a result, as shown in Fig. 1, the spacing of hoop ties formed from D16 reinforcing bars was roughly 15-30 cm.
In the damage survey immediately carried out after the earthquake, damaged piers were grouped into 5 damage categories from As (most severe damage) to D (minor or no damage). Ranking was according to the damage assessment procedure given in the Handbook for Roads Damaged by Earthquakes: Retrofit Procedure [7]. Of the 943 piers in the most severely affected 30 km section of the Kobe route, 15% were ranked as As or A, and 35% were B or C. Retrofitting of piers was carried out in two phases according to their level of damage: the top priority was to remove damaged piers and construct new piers; the next was to repair and strengthen existing piers. Piers ranked As and A were rebuilt. Those ranked B, C, and D were retrofitted. Footings were reused in both cases since they were found to be virtually unaffected by the earthquake in the detailed damage survey, which included use of a borehole camera.

Checking for the retrofit design was performed using the following three seismic levels:
① Level 1 (check for allowable stress using the seismic coefficient method prescribed in the 1990 Specifications for Highway Bridges) -
The design horizontal seismic coefficient on type II ground, on which the Kobe route is located, was 0.2 in the old standard, but it is 0.25 in the current standard.
② Level 2 (check for ultimate lateral strength prescribed in the same specifications) - Checks for ultimate lateral strength were not required under the old standard, but are needed under the current standard. The seismic intensity for checking is 0.85 on Type II ground.
③ Level 3-1 (check for ultimate lateral strength using the response spectrum method prescribed in the Retrofit Specifications)
Checking was done using the procedure given in the Specifications for Highway Bridges. However, the stress-strain curve of concrete and the seismic intensity used for checking were taken from the Reference for Application of Retrofit Specifications [8]. The shape of the stress-strain curve of concrete and the ultimate strain vary in accordance with the amount of reinforcement used for confinement. The seismic intensity for checking is 1.75 on Type II ground.
④ Level 3-2 (check by nonlinear dynamic analysis using seismic records taken at locations where the maximum acceleration was observed during the earthquake)
Wave form profiles representing each ground type, such as those recorded at the Kobe Marine Meteorological Observatory and JR Takatori Station, were used.

The typical cross section of a modified pier satisfying check levels ① and ② is shown in Fig. 1. The cross section is enlarged by 0.4-0.6 m from the original 3.2 m to 3.6-3.8 m. This cross section is then subjected to check level ③. If the energy conservation law is applied to the large design external force of the Kobe earthquake level, the ductility factor needed for ordinary RC piers will

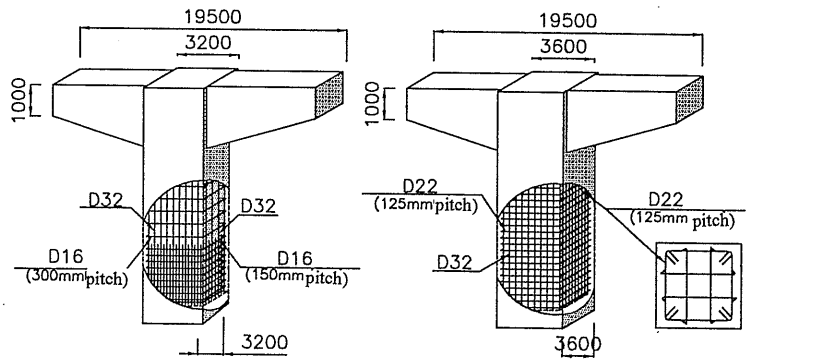

1) Dimension changes resulting from reconstruction
(left: existing; right: reconstruction)

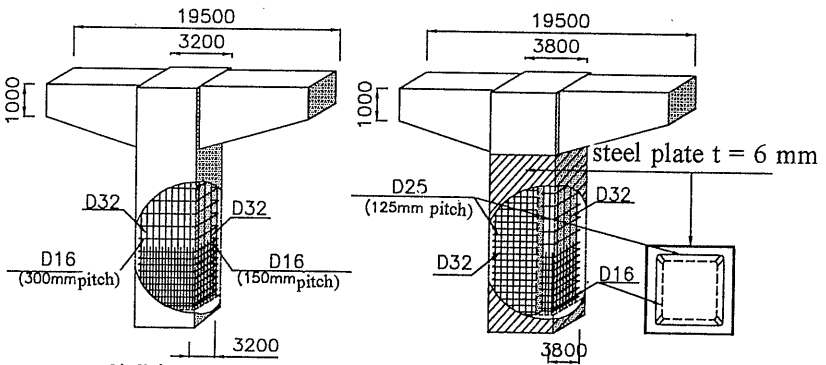

2) Dimension changes resulting from strengthening
(left: existing; right: strengthened)

Fig. 1 Configuration of piers

be approximately 6-8. This means that in the case of RC pier reconstruction, D22 hoop ties should be placed at a spacing of 125 mm and four intermediate hoops should be added to the cross section. In the case of strengthening, it means that D25 hoop ties should be placed at a spacing of 125 mm and the column should be jacketed in steel plate 6 mm thick. Since the required deformation strength is so high, we had to verify by experiment that the intended effect is duly achieved as a result of these retrofit measures.

3. EXPERIMENTAL PROGRAM

3.1 Outline

The specimens and parameters used in the experiments are given in Table 1. Figure 2 is a diagram giving details of the specimens. In the case of pier strengthening, the degree of damage to the pier before strengthening may cause variations in the overall strength of the pier after retrofitting. To evaluate this effect, four specimens were prepared, loaded up to two displacement levels to impose reinforcement damage (specimens of damage category B: up to 5 δ_y ; specimens of damage category C: up to 3 δ_y), and then strengthened by RC jacketing or a combination of steel + RC jacketing. In total, 15 specimens were produced in consideration of the design horizontal seismic coefficient and the anchoring method of the steel plate and reinforcement.
The design horizontal seismic coefficient (K_{hc}) given in Table 1 is obtained by the equation below, using the ultimate lateral strength (Pa), allowable ductility factor (μ) , and equivalent weight (W) of each specimen. This coefficient is used to check the ultimate lateral strength of a pier under seismic loading.

$$(K_{hc}) \cdot W = Pa \cdot (2\mu - 1)^{0.5} \qquad (1)$$

Specimens were prepared to 1/6 scale with a square cross section. The test set-up is shown in Fig. 3.

Table 1 Specimens and parameters for experiment

damage rank	specimen No.	strengthening	main reinforcement ratio (%) 1)	hoop tie ratio (%) 1)	designh horinzontal seismic coefficient (Khc) 1)	anchoring	remarks
	1	none (existing)	1.58	0.11	0.66	----------	C rank damage
	2					----------	
	3					----------	B rank damage
	4						
D	5	steel jacketing	2.05	0.64	1.28	post-installed resin anchors2) up to footing bottom	steel plate is anchored at the bottom
	6		1.58		1.20		Vg=0 (Vg:gap between steel plate and footing)
	7					----------	Vg=5 cm
B C	8	RC jacketing	1.63	0.60	1.84	post-installed resin anchors3)up to footing bottom	No.1 specimen after testing was reused Strengthening effect on C rank damage
	9					----------	No.3 specimen after testing was reused Strengthening effect on B rank damage
	10	Steel+RC jacketing		0.66	1.67	----------	No.2 specimen after testing was reused, Vz=5cm Strengthening effect on C rank damage
	11						No.4 specimen after testing was reused, Vz=5cm Strengthening effect on B rank damage
A As	12	RC reconstruction	1.63	0.27	1.21	Pre-installed main reinforcement3)up to footing bottom	standard specimen
	13					post-installed resin anochors3) up to footing bottom	
	14					post-installed resin anchors3) required anchoring length from footing face	
	12'			0.58	1.88	pre-installed main reinforcement3)up to footing bottom	

1) The valus is both existing and strengthened combined
2) The length is 1/2 of the footing thickness plus required anchoring length by calculation
3) The length is the thickness of cover concrete on the footing face plus required anchoring length by calculation

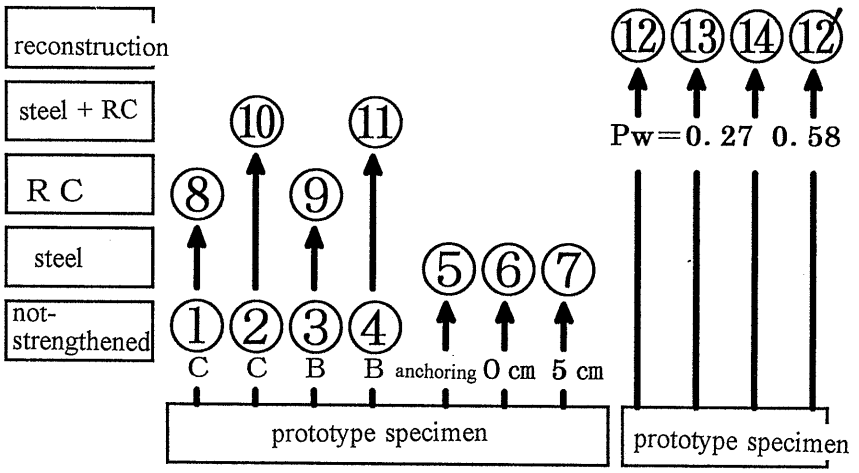

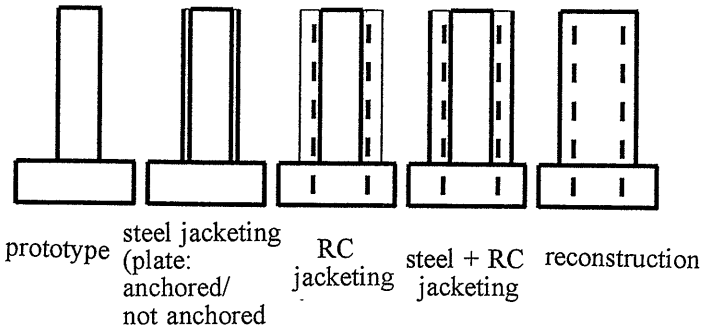

Fig. 2 Description of specimens

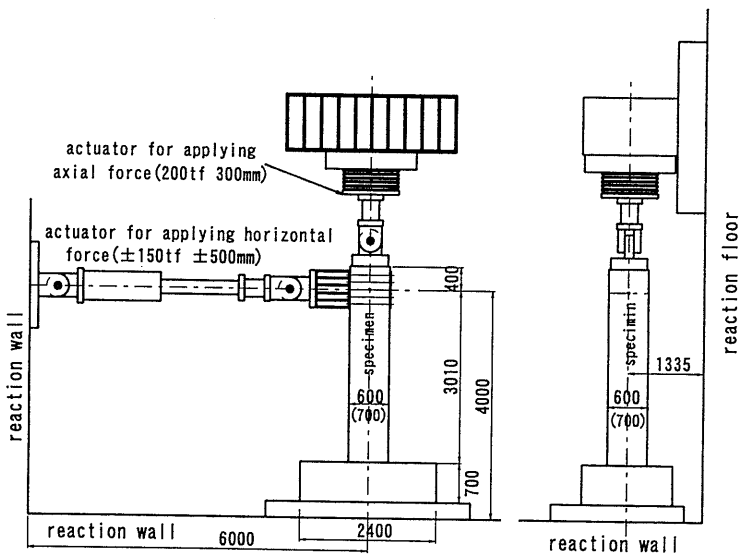

Fig. 3 Test setup

3.2 Configuration of specimens

① Specimens simulating damaged piers (Nos. 1, 2, 3, 4)
The dimensions of these specimens are given in Fig. 4. Shear reinforcement was placed at a ratio of 0.11%, because: (1) the purpose of this experiment was to assess the increase in bending strength; and (2) the average shear reinforcement ratio of real piers is 0.11%. The shear span ratio and the main reinforcement ratio were 5.0 and 1.58%, respectively, in accordance with the values for real piers. As to the main reinforcement and hoop ties, D 35 and D 16 reinforcing bars are used respectively in real piers. On the other hand, in these specimens with a cross section 60 × 60 cm, D10 and D6 bars, slightly larger than the bars in real piers in terms of cross sectional ratio,

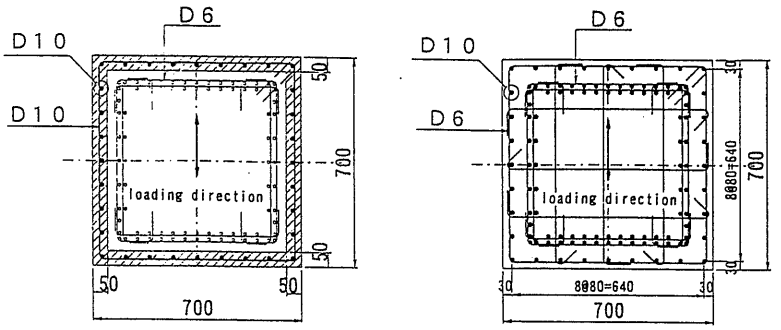

*No.10,11 were produced by covering a steel plate t=1.6mmover No8,9.
*No.12 and No.12' differ in that the spacing of hoop ties is 150 mm and 70 mm, respectively
No.1,2,3,4 do not have the shaded area seen in No.8,9.

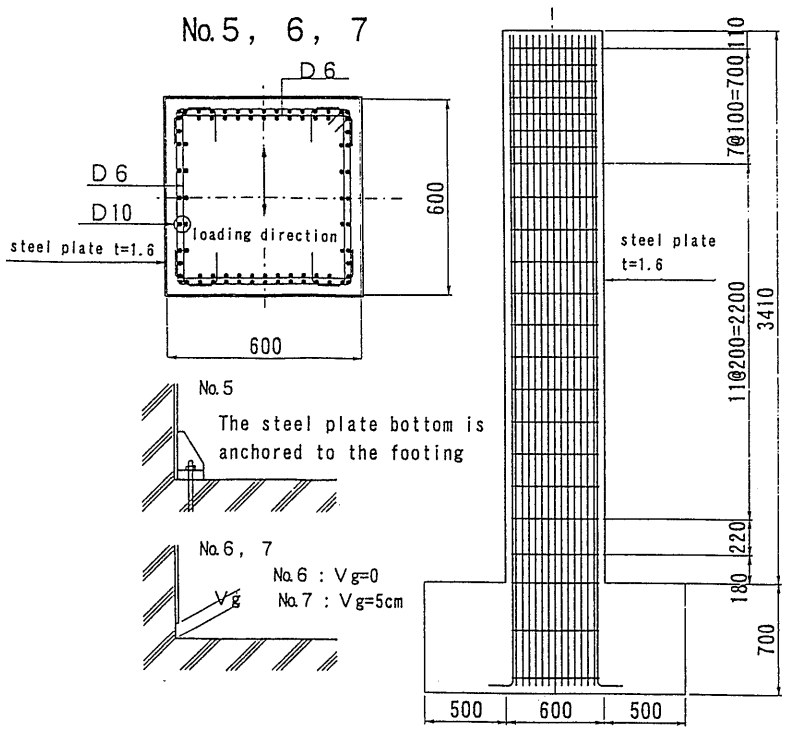

Fig. 4 Dimensions of specimen

were used, respectively. The main reinforcement was extended down to the footing bottom and anchored there, as in real piers.

② Specimens for steel jacketing (Nos. 5, 6, 7)
Steel jacketing specimens, which were clad in a steel plate using resin, were produced in three types. No. 7 specimen was prepared to have a 50 mm gap between the bottom end of the steel plate and the upper face of the footing. No. 6 specimen had no such a gap. No. 5 specimen was such that the steel plate was integrated with the footing by means of anchors driven through frames (steel plate: t=30 mm; rib: t= 4.5 mm). The thickness of the steel plate used for the specimens was 1.6 mm as 1/6 of 9 mm, thus averaging the actual plate thickness of real piers which is 6-12 mm.

③ Specimens for RC jacketing (Nos. 8, 9)
The intent is to reuse damaged piers by removing damaged concrete, replacing damaged reinforcement, and then placing new concrete. However, the replacement of damaged reinforcement is not always possible under all site conditions. Therefore, testing was carried out to evaluate the effect of reusing damaged reinforcement as is.
Specimens were loaded to impose B and C category damage and then, reusing the damaged reinforcement, the following repairs were carried out: In specimen No. 9 with B damage, resin was injected into the cracks, the covering concrete in the section up to 1.5 m from the column bottom was chipped away, and shrinkage-compensating mortar was applied. In the case of specimen No. 8 with C damage, epoxy resin was injected into the cracks, and then the main reinforcement was anchored to the existing footing by post-installed anchors. The anchorage length of the anchor bars was made 650 mm by summing the design anchorage length (30 Φ) and one half of the footing height. D10 hoop ties were then placed at a spacing of 40 mm and covered with shrinkage-compensating mortar.

④ Specimens for RC + steel jacketing (Nos. 10, 11)
Specimens No. 10 and 11, after loading to impose B and C category damage, respectively, were repaired and strengthened by RC jacketing in the same way as specimens No. 8 and 9. To increase lateral confinement, hoop ties consisting of D6 bars were placed at a spacing of 8 cm. A steel plate with a thickness of 1.6 mm was then placed around the column leaving a 50 mm gap above the upper face of the footing.

⑤ Specimens for RC reconstruction (Nos. 12, 13, 14, 12')
Reconstruction of RC piers is meant to increase the design horizontal seismic coefficient of Check Level 1 from 0.2 to 0.25, while reusing the existing footings. To confirm if this is attainable, tests were conducted on the enlargement of the column cross section from 60 × 60 cm to 70 × 70 cm and the integration of the column and footing by means of post-installed anchors. For these tests, four specimens were prepared: specimen No. 12 represents a monolithic RC pier and footing; No. 14 represents a pier whose main reinforcement is anchored to the required design anchorage length; No. 13 represents a pier with the required design anchorage length plus half the height of the footing, and made integral with the footing; No. 12' is a specimen identical to No. 12 except that the spacing of the D6 hoop ties is reduced from 150 mm to 70 mm.

3.3 Materials

The concrete used was ready-mixed concrete (nominal strength = 270 kgf/cm^2) made from high-early strength cement and aggregate with a size of G_{max} = 20 mm. The average compressive strength of the concrete was 385 kgf/cm^2 (modulus of elasticity = 2.80×10^5 kgf/cm^2). Shrinkage-compensating mortar was used for RC jacketing and concrete repairs. The average compressive strength of this mortar was 422 kgf/cm^2 (modulus of elasticity = 2.02×10^5 kgf/cm^2). The yield point of main reinforcement (D10), hoop ties (D6), and the steel jacketing plate was 3,900 kgf/cm^2, 3,300 kgf/cm^2, and 2,500 kgf/cm^2, respectively.

3.4 Loading and measurements

An axial force equivalent to the axial stress of each strengthening method (15.3 kgf/cm^2 for

specimens simulating existing pier and steel jacketing; 11.5 kgf/cm^2 for specimens for RC jacketing, steel + RC jacketing, and RC reconstruction) was applied to the column top with a hydraulic jack, while a concurrent cyclic horizontal force was applied from the side using an actuator. The test setup is shown in Fig. 3. The jack for applying axial force was attached to the loading frame via a sliding device. Since a swivel was utilized to apply the axial force to the column top, the level of force was kept constant, despite horizontal displacement of the column top.

Loading was applied by the load-control method up to the yield point, the load at which the main reinforcement in the outer-most layer reaches the analytical yield point. After reaching the yield load, three cycles of reversed load were applied at each multiple of yield-load displacement (δ_y) under displacement control. Loading was continued until the load dropped to 50% after passing the maximum load. Measurements included displacement at the loading point, the distribution of horizontal displacement in the longitudinal direction, the relative vertical displacement at the column bottom and the face of the footing, and the steel plate and reinforcement strain.

4. EXPERIMENTAL RESULTS AND DISCUSSION

4.1 Organization of results

An adjustment was made with regard to main reinforcement pullout caused by horizontal displacement at the loading point: the rotational displacement at the column bottom obtained in the experiment was assumed to have been caused by main reinforcement pullout and this rotational displacement was deducted from the amount of deformation. The value thus obtained was the pullout-adjusted reinforcement displacement. To be more specific, the adjustment was made by extrapolating from the measured reinforcement pullout at a displacement of 2 ~ 3 δ_y, assuming that pullout was linearly proportional to displacement at the loading point. The ratio of reinforcement pullout to yield displacement was 40% on average, and 25% at yield.

Regarding the definitions of yield displacement and ultimate displacement, which have a significant effect on the derivation of the ductility factor, the following were employed. Yielding of the cross section is the state when the centroid of the tensile reinforcement reaches the yield strain. Also, yielding of a member, the yield load, and the yield displacement were each assumed

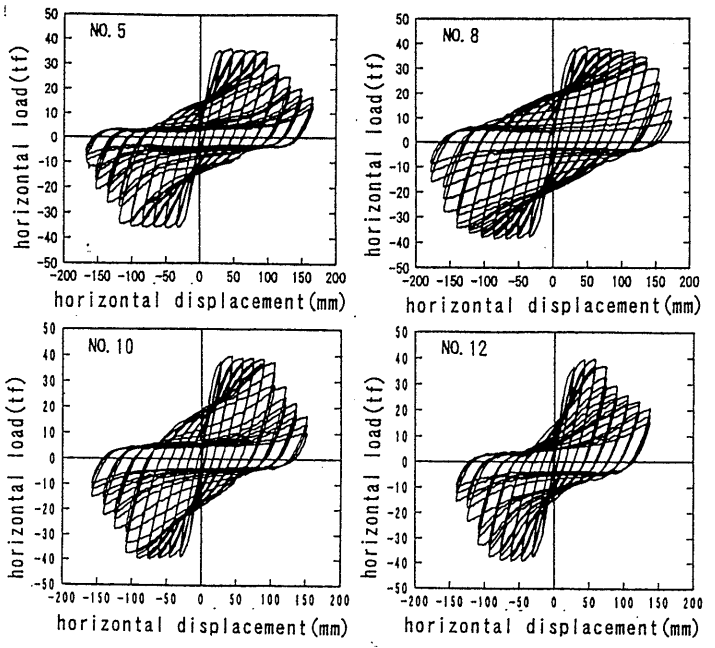

Fig. 5 Examples of load-displacement loop

to be the state when the cross section of the column bottom reaches yield, the calculated load at the time of yield, and the measured displacement under the yield load, respectively. The displacement at the time when the strength falls to 80% of the ultimate strength on the load-displacement envelop was considered the ultimate displacement. The value derived by dividing the ultimate displacement by the yield displacement was taken as the ductility factor.

4.2 Load-displacement relationship

Typical hysteresis loops describing the relationship between load and horizontal displacement at the loading point for the specimens are given in Fig. 5. Typical envelopes obtained from first-time loading at each reversed cyclic loading step are shown in Fig. 6. In this figure, reinforcement pullout is compensated for as described earlier. The load-displacement behavior of specimens No. 3, 5, 8, and 12 is described below.

No.3 specimen is a standard specimen loaded up to 5 δ_y until it suffered B level damage. In this specimen, horizontal cracks increased in the section 2 D (D = width of the cross section) above the footing face at the displacement of 2 δ_y (load : 24.9 tf). The specimen began to fracture at the column bottom at 4 δ_y (24.0 tf) and exhibited reinforcement buckling and a drop in maximum load at 5 δ_y (23.8 tf), leading to the ultimate state. The observed damage is illustrated in Fig. 7.
In specimen No. 5, the steel plate started to bulge at 2 δ_y (30.8 tf), cracks appeared on the steel plate around the connection with the frame at 4 δ_y (34.7 tf), the four corners of the plate above the frame tore in the direction of the main reinforcement at 6 δ_y (34.2 tf), and the load fell to 70 % of the maximum load at 8 δ_y (24.3 tf).

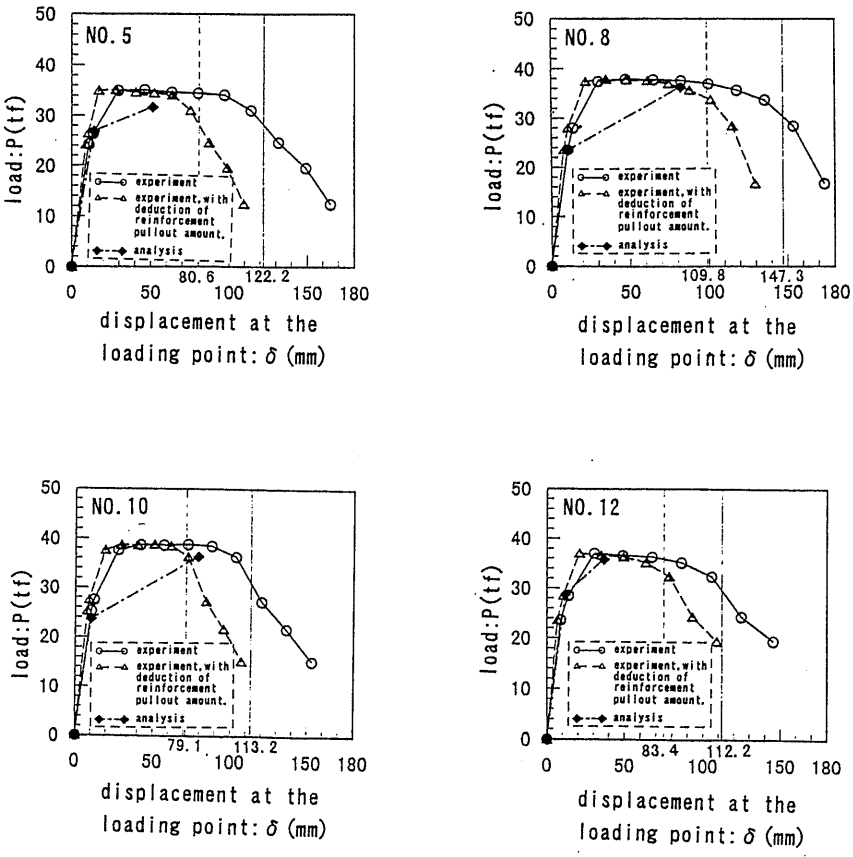

Fig. 6 Examples of load-displacement envelop

In specimen No. 8, cracks increased in number in the section 2 D above the footing face at 3 δ_y (37.9 tf) and buckling of the main reinforcement began at 7 δ_y (36.0 tf). The reinforcement began to fracture at 8 ~ 9 δ_y. Nine hoop ties fractured at 9 δ_y (29.3 tf) and the main reinforcement fractured at 10 δ_y. It is seen from Fig. 7 that the number of cracks in this specimen was much greater than in specimen No. 3, but the shear cracking observed in specimen

Table 2 Experimental and analytical results

specimen No.	main reinforcement ratio (%)	hoop tie ratio (%)	experimental results				analytical results				
			Py (tf)	δy (mm)	Pu (tf)	δu (mm)	Py (tf)	δy (mm)	Pu (tf)	δu (mm)	μ
1	1.58	0.11	20.6	16.6	24.3	51.7	—	—	—	—	—
2			19.8	16.6	24.3	51.4	—	—	—	—	—
3			20.8	16.8	24.7	87.6	—	—	—	—	—
4			20.1	16.7	24.7	87.6	—	—	—	—	—
5	2.05	0.64	27.0	16.4	35.1	122.2	26.8	14.1	31.7	51.0	3.6
6	1.58		22.9	17.2	26.0	92.5	19.5	13.2	23.8	63.1	4.8
7			23.1	17.2	25.0	94.9	19.7	12.9	24.0	61.1	4.7
8	1.63		28.1	17.0	37.9	147.3	25.0	12.2	36.3	81.8	6.7
9			27.4	17.0	38.8	96.3	25.0	12.2	36.3	81.7	6.7
10		0.66	27.8	15.0	38.8	113.2	25.1	12.1	36.4	75.2	6.2
11			26.6	15.0	38.7	94.8	25.0	12.4	36.1	77.9	6.3
12	1.63	0.27	28.7	18.4	37.0	112.2	28.8	11.7	35.8	36.5	3.1
13			29.5	18.4	37.4	128.0	28.8	11.7	36.1	36.5	3.1
14			31.1	18.4	37.5	118.1	28.8	11.3	36.1	36.6	3.2
12'		0.58	28.8	16.7	36.6	120.3	28.4	11.9	35.8	58.1	4.9

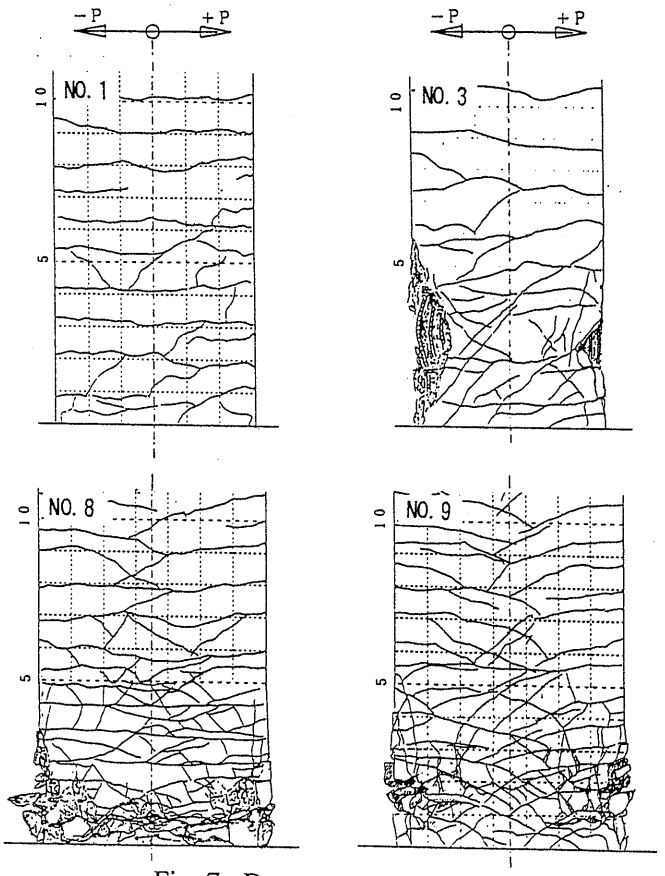

Fig. 7 Damage pattern due to loading

No. 3 was not found in this specimen.
In specimen No. 12, horizontal cracks began to increase in the section 1.5 D above the footing face at 3 δ_y (36.2 tf). Longitudinal cracks appeared at 6 δ_y (32.0 tf) and the main reinforcement fractured at 7 δ_y (23.8 tf).
As seen, all strengthened specimens were suffered bending failure before reaching fracture. Namely, horizontal cracks first appeared near the column end due to bending, then buckling of the main reinforcement followed, and finally fracturing of the main reinforcement occurred.

4.3 Comparison of maximum strength

The ultimate lateral strength of these specimens was calculated in accordance the Specifications for Highway Bridges and the Retrofit Specifications. The calculated values and experimental values are compared in Table 2 and Fig. 6. The material constants used for the calculations were the measured values. However, the modulus of elasticity of damaged reinforcement for damage levels B and C was taken to be Es = 2.1×10^6 kgf/cm^2 in calculating the ultimate state, and 2/3 Es in calculating the yield state based on the Handbook for Roads Damaged by Earthquakes: Retrofit Procedures [7]. As shown in Table 2, the maximum strength of specimens simulating existing piers was 24.3-24.7 tf, but this increased by 1.5 times to 36.6-38.8 tf in specimens strengthened by the three methods aside from steel jacketing. Among the specimens strengthened by steel jacketing, specimen No. 5, whose main reinforcement was anchored to the footing, showed a maximum strength of 35.1 tf, which is 1.4 times that of the non-strengthened pier. The ultimate load by calculation was approximately the same as the maximum strength obtained in the experiments.

4.4 Ductility factor

Figure 8 shows the ductility factor of each specimen, assuming that the displacement when the load dropped to approximately 80% of the maximum is regarded as the ultimate displacement. The ductility factors obtained in the experiments are all on the safe side as compared with those from analysis, even though an adjustment was made for the amount of reinforcement pullout. In particular, the experimental ductility factors for specimens No. 8 (RC jacketing) and Nos.12' and 13 (RC pier reconstruction) were all well over 8, which is far greater than the analytical ductility

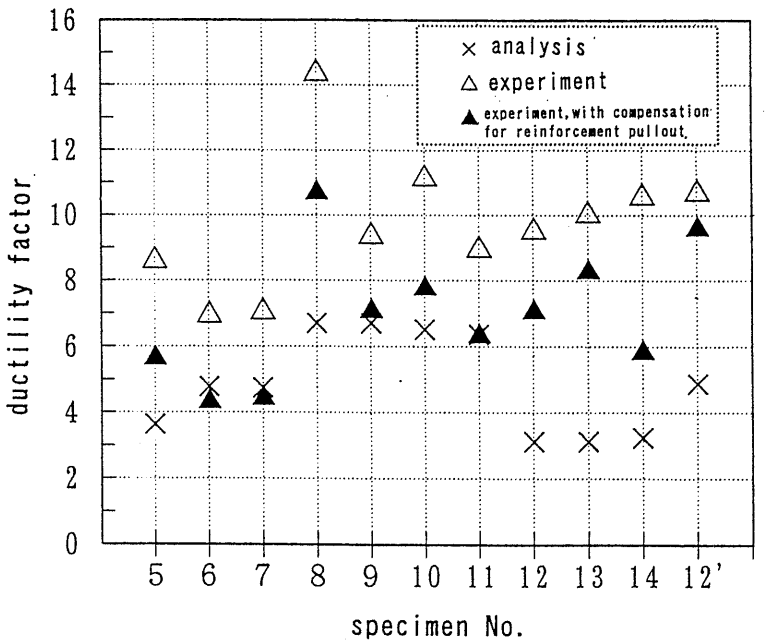

Fig. 8 Plot for ductility factor

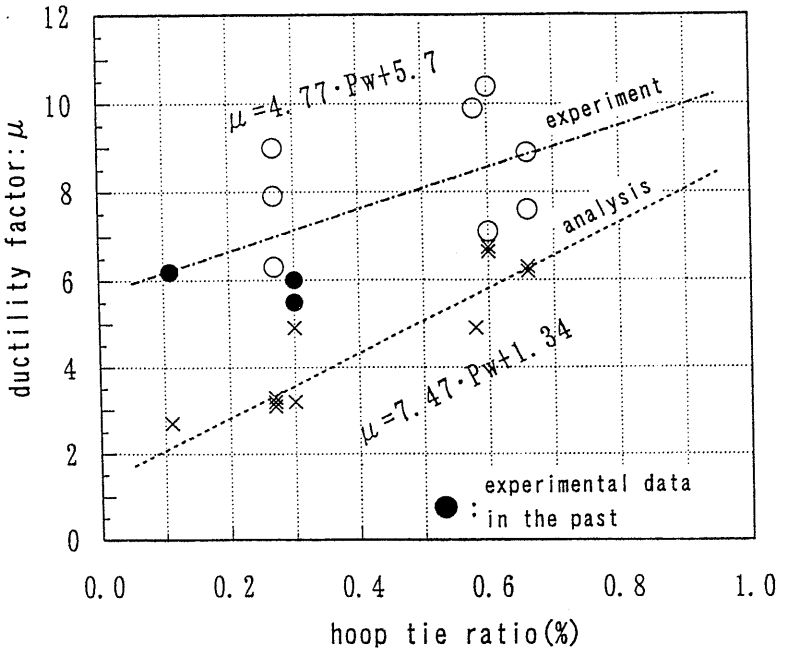

Fig. 9 Relationship between hoop tie ratio and ductility factor

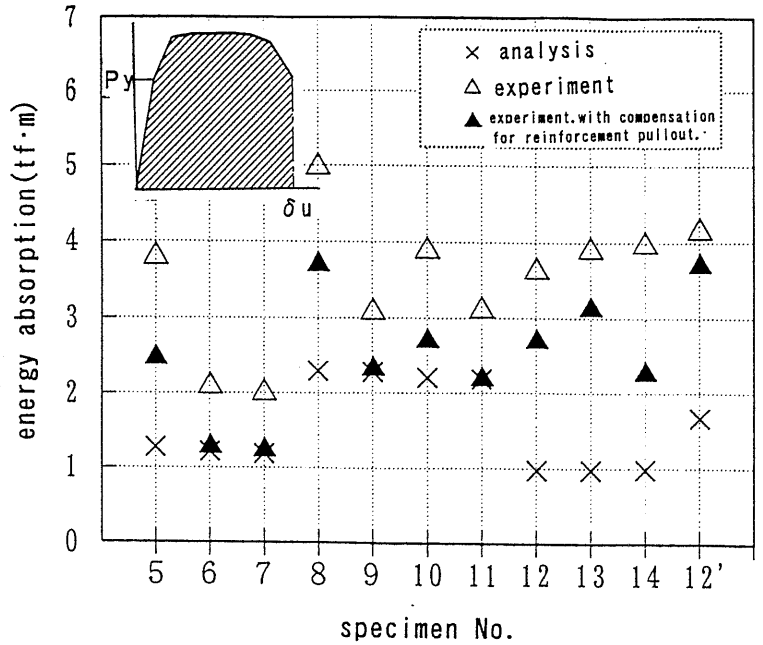

Fig. 10 Energy absorption up to ultimate displacement

factors. The reason for this is probably that the multi-layering of hoop ties and their excellent confinement effect were not properly evaluated in the analysis. Among the steel jacketed specimens, No. 5 (frame-anchoring type) was found to have a ductility factor well exceeding the analytical value. This means that anchoring via frames is effective not only in increasing strength but also in restraining main reinforcement buckling.

Figure 9 shows the relationship between hoop tie ratio and the ductility factor of RC jacketed specimens. The linear fit was obtained by the method of least squares. It is seen that the ductility factor increases from 6 to 9 in accordance with an increase in hoop tie quantity, indicating that an increase in hoop ties is an effective way to augment the ductility factor. It is also seen that the analytical ductility factor is approximately 3 when the hoop tie ratio is as small as 0.3%. This value of 3 is far below the experimental ductility factor, which is close to 6. However, it rises to about 7 as the hoop tie ratio increases to 0.6-0.7%. This is close to experimental ductility factor of 8. The reason is that in the case of ordinary RC piers the ductility factor of around 5 is readily secured because the type of shear fracture due to cyclic loading is the bending type, since the hoop tie ratio is around 0.2%. However, in the analysis based on the Retrofit Specifications, the ductility factor is evaluated for practical reasons from the ultimate strain induced by flexural compression. When the hoop tie ratio is as small as 0.2%, the ultimate strain is still small and hence the derived analytical ductility factor also remains small.
After passing this hoop tie ratio, the rise in ductility factor caused by the confining effect of hoop ties is slower in the experimental case than in the analytical case. However, the difference between the two values is within the acceptable range when the hoop tie ratio is 0.6-0.7%. As a whole, the experimental ductility factors are all on the safe side as compared with the analytical values up to a hoop tie ratio of 0.7%. However, from the above results and considering that the upper limit of hoop tie ratio is 0.7-0.9% in real piers, a ductility factor of 10 is probably the maximum for specimens with RC jacketing.

4.5 Energy absorption

The amount of energy absorption in each specimen, or the area of the load-horizontal displacement envelope, is given in Fig. 10. A roughly similar trend as ductility factor is found; namely, the experimental values are all larger than the analytical values. The difference is especially large in

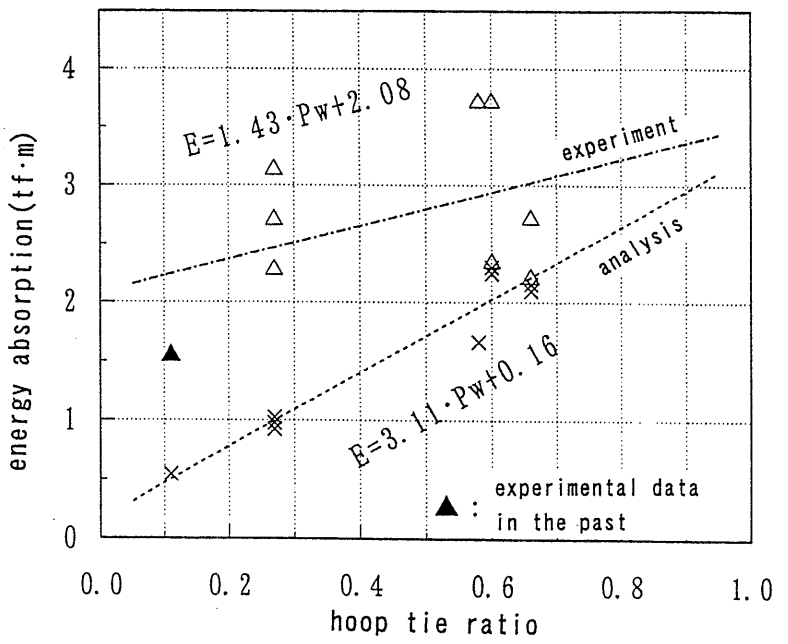

Fig. 11 Relationship between hoop tie ratio and energy absorption up to ultimate displacement

specimens Nos. 8 (damage category C), 13, and 12' (RC reconstruction). When specimens with B and C category damage are compared, it is clear that Nos. 9 and 11 (damage category B) has a smaller energy absorption area than Nos. 8 and 10 (damage category C). Figure 11 shows the relationship between hoop tie ratio and energy absorption derived from RC jacketed specimens. It is seen that the energy absorption area increases from 2.0 to 3.0 ft • m with rising hoop tie ratio, indicating that a higher hoop tie ratio is an effective way to increase the energy absorption. As noted above, a roughly similar tendency is found in the relationships between hoop tie ratio and both energy absorption and ductility factor. That is, when the hoop tie ratio is around 0.3%, the analytical value is considerably lower than the experimental value. When the ratio is 0.6-0.7%, the analytical value is in the range considered acceptable.

4.6 Evaluation of steel jacketing

Figure 12 shows a load-displacement envelope for specimens strengthened by steel jacketing. It is clear from this figure that specimen No. 5 with a steel plate anchored at the bottom is superior to the other specimens in maximum strength and deformation capacity. In contrast, specimens No. 6 and 7, which had a gap of 0 cm and 5 cm, respectively, between the bottom of the steel plate and

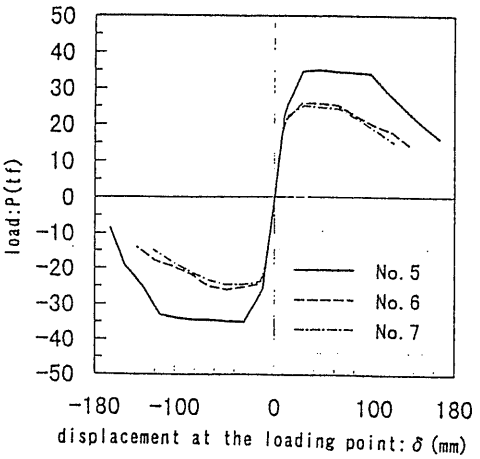

Fig. 12 Load-displacement envelop

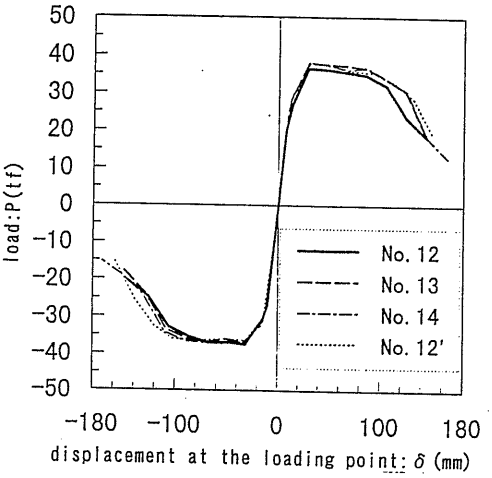

Fig. 13 Load-displacement envelop

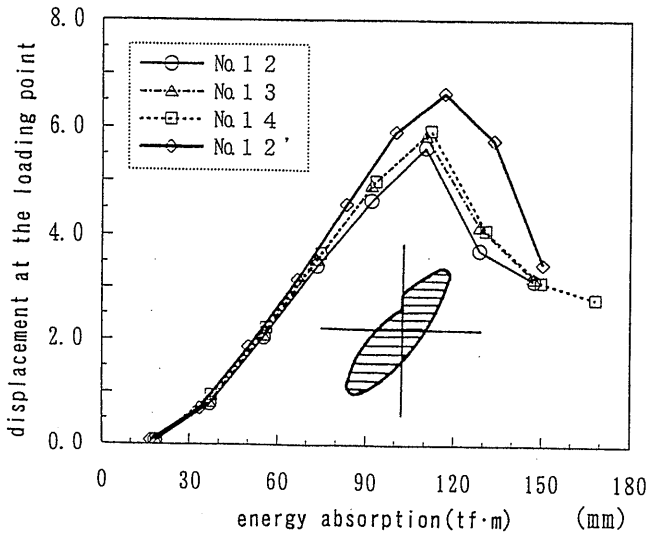

Fig. 14. Relationship between displacement at the loading point and energy absorption

the upper face of the footing, no conspicuous difference was observed in maximum strength and deformation capacity, suggesting that a gap around the bottom of the column leads to no substantial effect.

4.7 Evaluation of pier reconstruction

Shown in Fig. 13 is a load-displacement envelope obtained from specimens for RC pier reconstruction. When specimens No. 12, 13, and 14 are compared, no obvious difference is observed in ductility and no fractures are found around the anchors, indicating that the anchor is never a soft spot in earthquake loading. Figure 14 shows the relationship between displacement at the loading point and energy absorption. The energy absorption in this figure is the area encircled by the load-displacement hysteresis loop obtained from the second loading cycle. As is clear in Figs. 13 and 14, there is a tendency for the load to begin decreasing gradually from 5 δ_y (load: 34.8-36.7 tf) in all these specimens. On the other hand, in specimen No. 12' where the hoop tie ratio is higher than in the other specimens, the load begins to decrease from 6 δ_y (load: 35.2 tf). This specimen also had the same energy absorption as the other specimens at a displacement around 8-9 δ_y (150 mm), but the area enclosed was larger than the other specimens when the

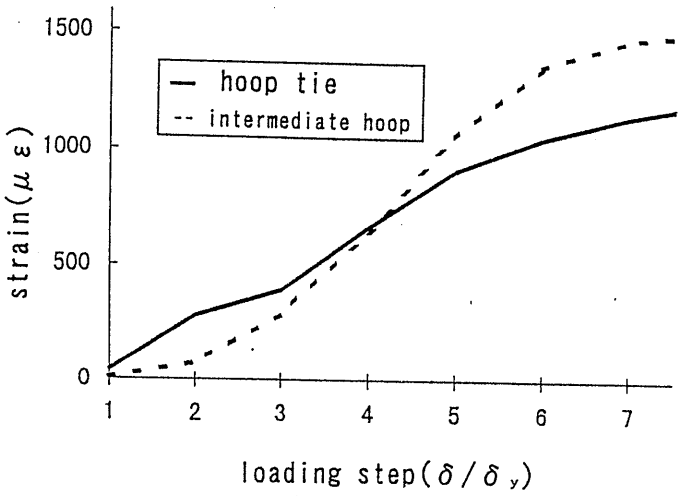

Fig. 15 Relationship between strain and loading cycle

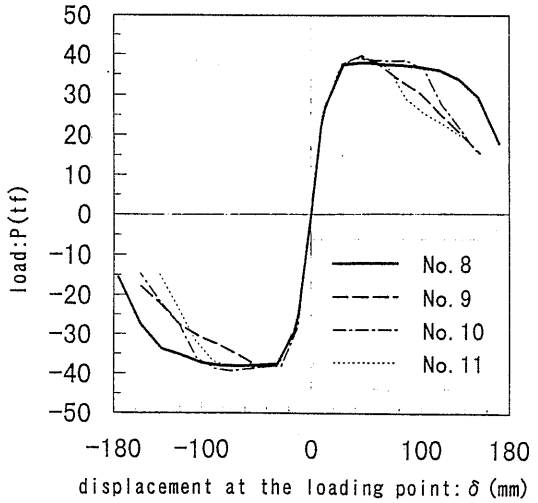

Fig. 16 Load-displacement envelop (No. 8, 9, 10)

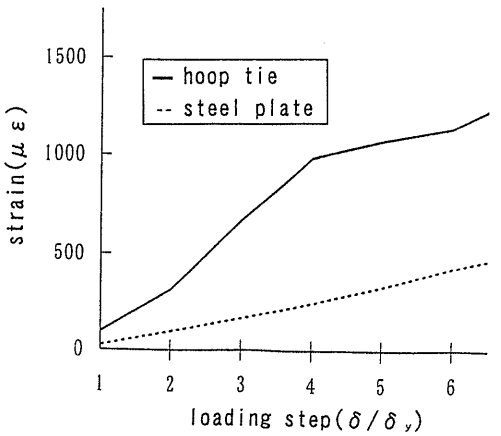

Fig. 17 Relationship between strain and loading cycle (No.10)

displacement was between 6 and 8 δ_y. This also indicates that an increase in hoop tie ratio contributes to better energy absorption at around point of the ultimate displacement. Figure 15 shows the strains of hoop ties and intermediate hoops observed in specimen No. 12'. The strains of these hoops continued to increase up to the yield strain with the load rose, showing that such hoops effectively increase the energy absorption.

4.8 Evaluation of damage strengthening

Figure 16 shows load-displacement envelopes obtained from specimens with B and C category damage that had been strengthened. Specimens No. 9 and 11 with category B damage exhibited the same level of maximum strength as Nos. 8 and 10 specimens with C damage, but the load fell quicker than with the latter specimens. This is probably because reinforcement of the B damage specimens had already buckled and bulged under initial loading and hence the addition of a compression force through continued loading easily leads to deformation in the horizontal direction. In contrast, in the specimens with C category damage, the same level of ductility and energy absorption as with specimen No. 12' was secured and hence the effect of damaged reinforcement may have remained slight. Given in Fig. 17 is the distribution of strain taken from the hoop ties and steel plate of specimen No. 10. It is clear from this figure that hoop tie strain increases rapidly with increased loading, but the increase in steel plate strain is gradual.
However, in terms of ductility factor and energy absorption, specimens with RC + steel jacketing and reconstructed RC specimens have roughly identical values, leading to the conclusion that there is no quantitative difference in their capacities when their hoop tie ratios are little different.

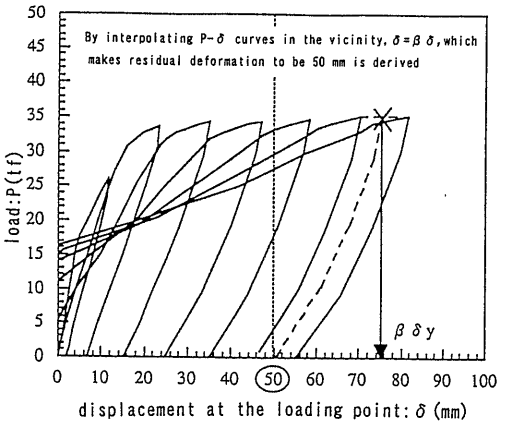

Fig. 18 Estimation of residual deformation

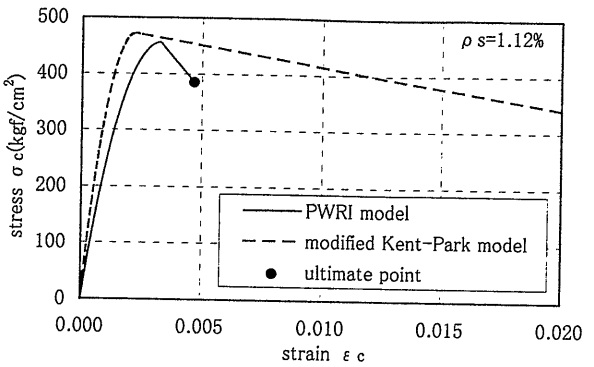

Fig. 19 Stress-strain model for concrete (No. 8)

Table 3 Modulus of plasticity derived from residual deformation

specimen No.	at yielding (experimental value) δy(cm)	Py(tf)	at residual displacement=50mm δu(cm)	Pu(tf)	modulus of plasticity :μ
3	1.68	20.7	8.06	24.7	4.8
4	1.67	19.5	8.45	24.7	5.1
5	1.64	27.0	8.17	37.8	5.0
6	1.72	22.9	7.84	24.3	4.6
7	1.72	23.1	7.81	23.0	4.5
8	1.70	28.1	8.50	38.3	5.0
9	1.70	27.4	8.75	33.4	5.1
10	1.50	27.8	8.36	39.6	5.6
11	1.50	26.6	8.25	35.6	5.5
12	1.84	28.7	8.64	36.3	4.7
13	1.84	29.5	8.53	37.4	4.6
14	1.84	31.1	8.17	37.8	4.4
12'	1.67	28.8	8.45	36.7	5.1

4.9 Evaluation of residual deformation

To resist large seismic forces, besides securing enough ductility and strength, it is necessary to contain the residual deformation of structures to a minimum such that normal traffic is not interrupted. Since detailed analysis of residual deformation has already been made by other researchers [14], we focused on the qualitative relationship between ductility factor and residual deformation.

As seen in Fig. 18, the displacement (δ) was obtained by extrapolating load-displacement envelopes which leave a residual specimen deformation of 50 mm. This value of 50 mm is the value which causes 300 mm of residual deformation at the column top of a real pier when the effect of deformation due to reinforcement pullout is neglected. It is also the value which causes approximately 200 mm of residual deformation at the body of a real pier after adjustment is made for the amount of reinforcement pullout. Next, by dividing the obtained displacement (δ) by δ_y, an allowable ductility factor corresponding to the amount of residual deformation is derived. Shown in Fig. 3 is the allowable ductility factor for each specimen when the residual deformation is allowed to be 50 mm. All are in the range 4.5-5.5, equal to about 60% of the ultimate ductility factor of each specimen.

5. ANALYTICAL INVESTIGATION

5.1 Outline

Parameter analysis was carried out to determine a suitable calculation method able to express the load-displacement relationship, as needed to check the seismic ultimate lateral strength of the piers. Then, the analytical and experimental results were compared to evaluate the effect of each parameter.
There are several definitions of ultimate displacement used in deriving the ductility factor of an RC column. It can be considered the horizontal displacement at the time when the strength falls to

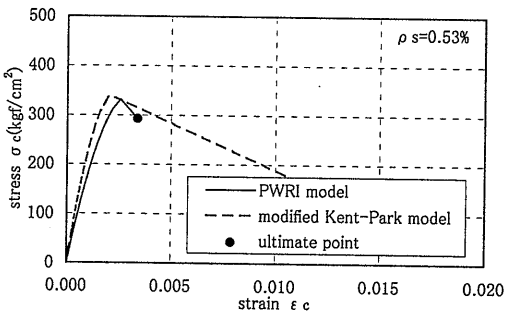

Fig. 20 Stress-strain model for concrete (No.12)

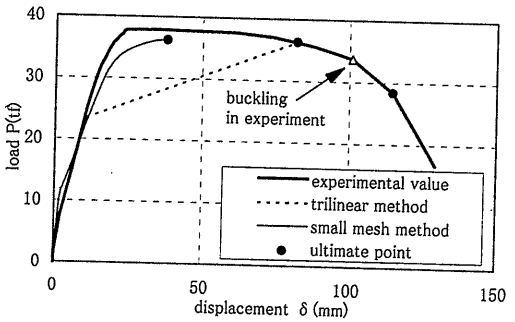

Fig. 21 Load-displacement relationship (No.8)

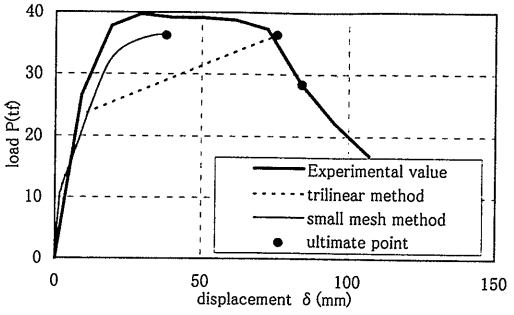

Fig. 22 Load-displacement relationship (No.10)

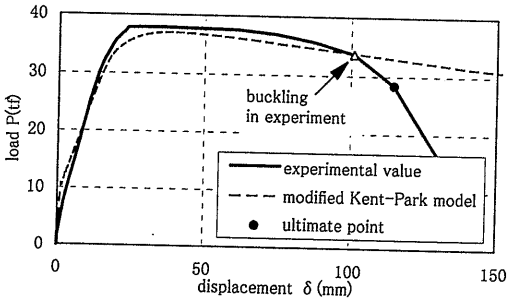

Fig. 23 Load-displacement relationship by small mesh method (No.8)

a calculated yield load, or at the time when the horizontal strength begins to drop from a stable value near the maximum strength. Alternatively, some call the displacement at the time when the applied load does not fall below 80% of the maximum load the critical displacement. To define the ultimate displacement of the column in the region of strength loss and analyze it, it is necessary to estimate the actual curvature distribution of the column by modeling the M-Φ relationship after buckling or fracturing of the reinforcement. By integrating this in the longitudinal direction, the load-displacement relationship at the ultimate state can be estimated. However, since it is not that simple to account for the mechanism of reinforcement buckling or fracturing, the point where buckling of the main reinforcement begins was regarded as the onset of the ultimate state.

5.2. The trilinear and small mesh methods

In checking the ultimate seismic lateral strength based on the Retrofit Specifications, the forces acting on each cross section of the column are first derived from the stress-strain relationships of concrete and the reinforcement, then the moment and curvature at crack initiation, yielding, and onset of the ultimate state are derived at each cross section from the balance of forces. Next, assuming the moment-curvature relationship of those three points to be linear (and thus providing the curvature distribution in the column longitudinal direction), the relationship is integrated twice to derive the displacement at the column top at the yield and the ultimate state. This is called the trilinear method.

In the current analysis, the yield point for calculation purposes was assumed to be the point at which strain at the centroid of the tensile reinforcement reaches the yield strain, and the ultimate point was assumed to be the point at which concrete at the compression fiber reaches the ultimate strain defined by the Retrofit Specifications.
In addition to this, there is another method for estimating displacement at the column top. This entails providing sequential moment-curvature relationships of the cross section derived from calculation as the curvature distribution in the column longitudinal direction, and integrating this distribution. This is called the "small mesh" method. The relations between these two analysis methods and the load-displacement relationship are investigated below.

5.3 Stress-strain model for concrete

Two models, the PWRI model and the modified Kent-Park model, were compared to find which was most appropriate as a stress-strain model for concrete. Examples of the concrete stress-strain relationship are shown in Figs. 19 and 20. The PWRI model given in the Retrofit Specifications uses a stress-strain relationship with parameters consisting of the compression strength of concrete F'_c, the volumetric ratio of steel for lateral confinement ρ s, and the yield strength f_y. This model was derived from compression test data during the period of stress reduction from the maximum to 50% [9][10]. In contrast, in the modified Kent-Park model, the value defined as the ultimate strain in the PWRI model is not used, though the increase in concrete compressive strength arising from the confinement effect is duly taken into account [11]. As seen in Fig. 20, when the ratio of lateral confinement reinforcement is large, the stress decrease after the peak is rather gentle in the modified Kent-Park model compared with that of the PWRI model. Also, the modified Kent-Park model cannot be applied to the analysis of steel jacketing because it requires the spacing of the lateral confinement reinforcement as a parameter. For the stress-strain relationship of the reinforcement, the perfectly elasto-plastic model specified in the Retrofit Specifications was used. The yield strength adopted was 3,900 kgf/cm^2 based on tensile test results.

5.4 Effect of analysis method

A comparison of the load-displacement relationship obtained by experiment and calculation for specimens No. 8 and 10 after deducting the amount of reinforcement pullout is given in Figs. 21 and 22, respectively. The PWRI model was used to calculate the stress-strain relationship of the concrete, and the trilinear and small mesh methods were used for displacement. From these figures, it is seen that the ultimate displacement derived by the combination of the PWRI model and the trilinear method is closer to the experimental ultimate displacement than that obtained with

the PWRI model and the small mesh method.

5.5 Applicability of the small mesh method

The above investigation demonstrated that the combination of the PWRI model and the small mesh method was not suitable for estimating the ultimate displacement. Next, the applicability of a combination of the modified Kent-Park model and the small mesh method was investigated. Figures 23, 24, and 25 compare the experimental and calculated load-displacement relationships for No. 8, 12', and 12, respectively, in the case of using the small mesh method. Here, the experimental and calculated results are in relatively good agreement up to the onset of main reinforcement buckling. Therefore, we extended the calculation. First, the displacement at the onset of main reinforcement buckling was obtained from the experimental results, and then the concrete strain at the compression fiber (ε_{bk}) at the time of this was calculated by the small mesh method. The relationship between the calculated concrete strain and the confinement index given by the modified Kent-Park model ($K=1+\rho_s \cdot f_{yh} / f'_c$) is shown in Fig. 26. Though a quantitative evaluation is difficult to make because the number of specimens to which the modified Kent-Park model is applicable is very small, the concrete strain at the compression fiber (ε_{bk}) is 32,000 μ in specimen No. 12 with small confinements and 42,000-47,000 μ in specimens No. 8 and 12' with large confinements. From this, it can be said that there is a correlation between the compressive strain of concrete and the confinement index at the time of main reinforcement buckling.

6. EVALUATION BY FIBER MODEL

6.1 Outline

Nonlinear RC analysis was used to carry out a quantitative evaluation of the strengthening effect on damaged piers. A fiber model in which the cross section was divided into a number of elements was employed to model a beam. Frame analysis based on beam theory was adopted for structural analysis. As the stress-strain model of the concrete, the modified Muguruma-Watanabe model was used, and as the stress-strain model of the reinforcement, the GMP model was utilized.

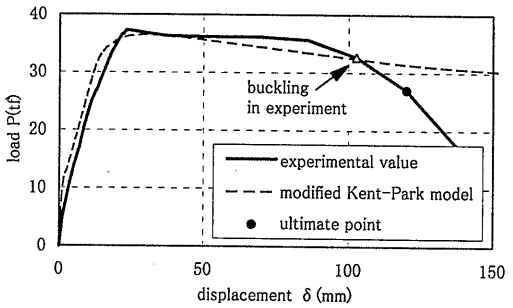

Fig. 24 Load-displacement relationship by small mesh method (No.12')

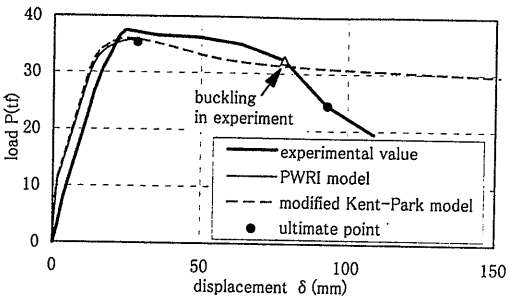

Fig. 25 Load-displacement relationship by small mesh method (No.12)

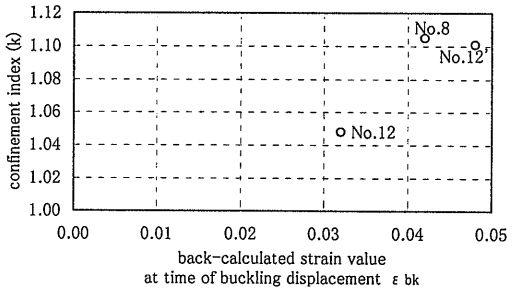

Fig. 26 Relationship between confinement index and back-calculated strain value

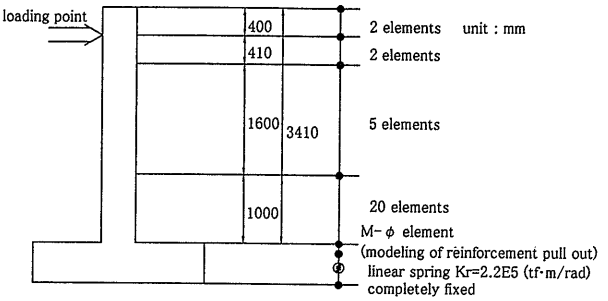

Fig. 27 Analysis model

The analysis followed the procedure given in References 12 and 13. As parameter (R_0) for evaluating the Bauschinger effect, though 20.0 is generally recommended, 15.0 was chosen in the current analysis because the type of loading was reverse cyclic [12]. The following two cases were analyzed:

a) The analysis model was specimen No.1. Analysis was conducted up to 5 δ_y, and the damage at 3 δ_y was evaluated.

b) The analysis model was specimen No. 8. Analysis was carried out up to 7 δ_y, and damage up to this displacement was compared with that obtained in the experiment.

The analysis model simulating specimen No. 1 is shown in Fig. 27. A linear rotational spring simulating the rigidity of the column and a nonlinear rotational spring simulating the pullout of the main reinforcement (based on the Muto rule) were fitted to the column end. The model structure was a column, 3.41 m in height, with a square cross section of 60 × 60 cm. All components were modeled with nonlinear elements, and there was a total of 29 elements and 30 nodal points. The cross section was divided into 50 fibers. All reinforcement, including double reinforcement and side reinforcement, was modeled. The initial axial stress was a load of N=55.08 tf applied in the direction perpendicular to the column. The same model was used for specimen No. 8 except that the cross section was enlarged to 70 × 70 cm. The physical properties of these specimens are shown in Tables 4 and 5. The second gradient of reinforcement was 2% of the initial gradient.

6.2 Analytical results

① Specimen No. 1

Figure 28 shows a load-displacement loop at the loading point on the column top taken from

Table 4 Physical properties (No. 1)

Concrete	
Initial Young's modulus	2.75×10^{6} tf/m^2
Yield strength	3650.0 tf/m^2
Yield strain	2000×10^{-6}
Tensile strength	257.0 tf/m^2
Reinforcement	
Initial Young's modulus	2.1×10^{7} tf/m^2
Yield strength	38900.0 tf/m^2
Second gradient	2.1×10^{5} tf/m^2

Table 5 Physical properties (No. 8)

Concrete	
Initial Young's modulus	1.99×10^{6} tf/m^2
Yield strength	4250.0 tf/m^2
Yield strain	2000×10^{-6}
Tensile strength	314.0 tf/m^2
Reinforcement	
Initial Young's modulus	2.1×10^{7} tf/m^2
Yield strength	38900.0 tf/m^2
Second gradient	2.1×10^{5} tf/m^2

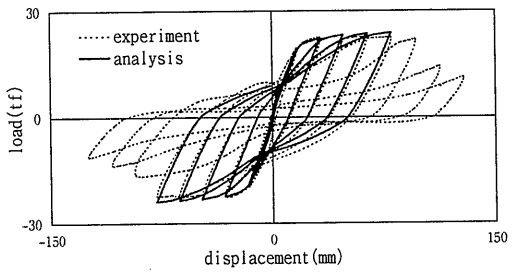

Fig. 28 Load-displacement loop at loading point (No.1)

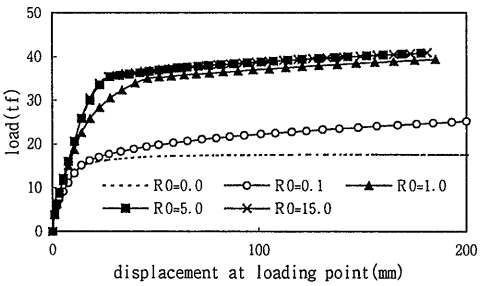

Fig. 29 Analytical result for displacement by monotonic loading

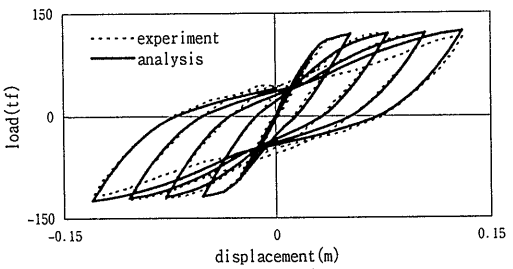

Fig. 30 Load-displacement loop at the loading point (No.8)

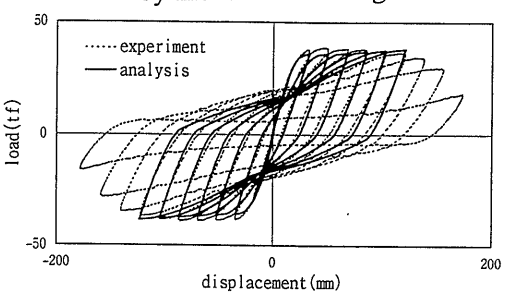

Fig. 31 Load-displacement loop at the loading point (specimen designed by the 1970 Specification)

specimen No. 1. Though three cycles of loading were completed at each displacement amplitude, only the load-displacement loop from the first cycle is shown in the figure. The damage incurred at 3 δ_y was approximately R=2.0 at the reinforcement in the outer-most layer and about 65% on the first gradient. Then, using specimen No. 8, sensitivity analysis was carried out by monotonic loading, assuming that the incurred damage equaled the average decrease in R_0 of the reinforcement. The results of this analysis are given in Fig. 29. The analytical results show that a decrease in R_0 of the reinforcement does not affect the overall strength of a strengthened pier if $R_0 \geqq 2.0$.

② Specimen No. 8
In the analysis of this specimen, R_0=15.0 was employed based on the damage evaluation of the reinforcement above. Figure 30 shows a load-displacement loop at the loading point on the column top. For comparison, the analytical results for a standard pier built in accordance with the Specifications for Highway Bridges, 1980 are shown in Fig. 31 [12].

6.3 Discussion

① Evaluation of analytical results
Both analytical and experimental results of specimens No. 1 and 8 are in good agreement until the load-displacement loop starts to lose its steep inclination. This result is the same as noted in References 12 and 13. From a quantitative evaluation of the strengthening of specimen No. 1, it was confirmed that the damage incurred at 3 δ_y was not harmful to the overall performance of the column after strengthening.

② Comparison with a pier built according to the 1980 standard
Analytical results derived from specimens No. 1 and 8 were roughly similar to those shown in Reference 12. However, as compared with a standard pier designed by the Specifications for Highway Bridges of 1980, the rigidity of the rotational spring at the area of reinforcement pullout is relatively small in these specimens compared with the column rigidity. This is probably for such reasons as measurement fluctuations affected by experimental conditions, differences in specimen size, and differences in loading cycles. As a result, the effect of plastic deformation in the area of reinforcement pullout was larger in the current analysis as compared with the results from the 1980 pier given in Fig. 31, and the load-displacement loop is rather linear. Other than this, no conspicuous difference was found.

7. CONCLUSIONS

Experiments were conducted and a method of analysis developed to evaluate the effectiveness of four strengthening methods proposed for expressway piers built by the 1964 design standard and damaged by the 1995 Kobe Earthquake. These four strengthening methods were steel jacketing, RC jacketing, a combination of RC and steel jacketing, and RC reconstruction. The following conclusions were drawn from the results:
① In reversed cyclic loading tests, it was found that all strengthened specimens had gained considerable deformation capacity compared with the unstrengthened state.
② When specimens of RC reconstruction (one with the main reinforcement anchored to the footing by post-installed anchors; the other with monolithic main reinforcement and footing requiring no post-installed anchors) were compared, no visible difference was found in the fracture mode, strength, and deformation capacity. From this, it can be said that anchoring with by post-installed anchor bars does not constitute a weak point against earthquake loading.
③ Checks of ultimate lateral strength using the PWRI model as designated in the Retrofit Specifications yielded safer values as compared with the experiments. However, it was noted that the increase in ductility factor became rather gradual as the hoop tie ratio was increased, suggesting that there may be an upper limit to the hoop tie ratio.
④ Of three specimens made to test steel jacketing, the one with the steel plate anchored at the base and confined by frames exhibited a substantial increase in strength and deformation capacity, exceeding the level required by the Retrofit Specifications. In contrast, the remaining two specimens in which the steel plate was confined only in the horizontal direction yielded an increase in strength and deformation capacity to the level required by the Retrofit Specifications.

⑤ Specimens of RC reconstruction all demonstrated a considerably higher deformation capacity than required by the Retrofit Specifications. This is probably because the lateral confinement of reinforcement is evaluated conservatively in the Retrofit Specifications.
⑥ Specimens with category B damage (loaded up to 5 δ_y) and strengthened by RC jacketing and steel + RC jacketing had approximately the same maximum strength as specimens with category C damage (loaded up to 3 δ_y) and strengthened by the same methods. However, the deformation capacity of the former specimens was slightly smaller than that of the latter, because the load decrease after reaching the maximum was rather quicker in the former. The reason for this is probably that, if buckled reinforcement is reused without repair, it tends to deform in the horizontal direction when subjected to compression forces as a result of loading.
⑦ Calculated load-displacement relationships derived from the small mesh method plus both the modified Kent-Park model and the PWRI model were in good agreement with the experimentally obtained load-displacement relationship up to the peak load. Also, the calculated load-displacement relationship derived from the small mesh method and the modified Kent-Park model showed good correlation with the experimental load-displacement relationship up to the onset of reinforcement buckling.
⑧ Simulation analysis was conducted on the experimental results by employing an RC nonlinear analysis technique based on a fiber model. The pullout ratio of main reinforcement was taken into account as a nonlinear rotational spring. From these results, it was found that a fiber model can satisfactorily simulate the load-displacement relationship up to the onset of main reinforcement buckling, even in a specimen with a high deformation capacity.

REFERENCES

[1] Hayashi, H., "Retrofit Design of Hanshin Expressway Kobe Route", Doboku-Seko (Technical Journal), Vol.36, No.12, pp. 71-76, 1995.11 (in Japanese)
[2] Committee for Retrofit of Road Bridges Damaged by Kobe Earthquake, "Specifications for Retrofit of Road Bridges Damaged by Kobe Earthquake", 1995.2 (in Japanese)
[3] Machida, A., Mutsuyoshi, H., and Toyota, K., "Analytical Study on Ultimate Displacement of RC Piers", Proc. of JSCE, V-6, No.378, pp. 203-212, 1987.2 (in Japanese)
[4] Osaka, Y., Suzuki, M., Kuwasawa, S., and Ishibashi, T., "Studies on the Restoring Characteristics of RC Columns under Static Cyclic Loading", Proc. of JSCE, V-5, No.372, pp. 45-54, 1986.2 (in Japanese)
[5] Nakamura, H., Niwa, J., and Tanabe, T., "Analytical Evaluation of the Ductility of RC Members", Proc. of JSCE, V-16, No.442, pp. 127-135, 1992.2 (in Japanese)
[6] Kawashima, K., Unjo, Sugita, and Nakajima, "Evaluation of Seismic Performance of Reinforcement Cut-off on RC piers and Seismic Strengthening, Technical Report of Public Works Research Institute, Ministry of Construction, No. 189, 1993.9 (in Japanese)
[7] Road Association of Japan, "Handbook for Roads Damaged by Earthquakes: Retrofit Procedure", 1988.2 (in Japanese)
[8] Road Association of Japan, "Reference for Application of Retrofit Specifications", 1995.6 (in Japanese)
[9] Hoshikuma, J., Kawashima, K., and Nagaya, K, "Stress Strain Model for Reinforced Concrete Columns Confined by Lateral Reinforcement", Proc. of JSCE, V-28, No.520, pp. 1-11, 1995.8 (in Japanese)
[10] Hoshikuma, J., Kawashima, K., and Nagaya, K, "Compressive Loading Test on Confined Concrete Column Using Large Scale Model and their Stress-Strain Characteristics", Doboku-Gijyutu Shiryo (Engineering Reference), Vol.37, No.7, pp. 32-37, 1995.7 (in Japanese)
[11] Park, R. and Priesley, N., "Ductility of Square Confined Concrete Columns", Journal of Structural Division, Proc. of ASCE, Vol.108, No. ST.4, pp. 929-950, 1982.4
[12] Ukon, H. Kosa, K., Inoue, S., and Yoshizawa, Y., "Nonlinear Simulation Analysis Using Fiber Model for Cyclic Loading Test on Standard Pier", Proc. of JCI, Vol.17, No.2, 1995.6 (in Japanese)
[13] Kosa, K., Kobayashi, K., Murayama, Y. and Yoshizawa, Y., "Experimental Study on Reversed Load-Displacement Behavior of RC Pier by Large Scale Model Tests", Proc. of JSCE, V-31, No.538, pp. 47-56, 1996.5 (in Japanese)
[14] Kawashima, K., Macrae, G., Hoshikuma, J., and Nagaya, K., "Residual Displacement Response Spectrum and Its Application", Proc. of JSCE, I-29, No.501, pp. 183-192, 1994.10 (in Japanese)